Supplementary Information

Tuning Mobility and Stability of Lithium Ion Conductors based on Lattice Dynamics

Sokseiha Muy,[1] John C. Bachman,[2] Livia Giordano,[2,3] Hao-Hsun Chang,[4] Douglas L. Abernathy,[5] Dipanshu Bansal,[5] Olivier Delaire,[5,6] Hori Satoshi,[7] Ryoji Kanno,[7] Filippo Maglia,[8] Saskia Lupart,[8] Peter Lamp, [8] Yang Shao-Horn[1,2,4]

[1]Department of Materials Science and Engineering, [2]Department of Mechanical Engineering, Massachusetts Institute of Technology, Cambridge, Massachusetts 02139, US.

[3]Dipartimento di Scienza dei Materiali, Università di Milano-Bicocca, 20126 Milano, Italy.

[4]Research Laboratory of Electronics, Massachusetts Institute of Technology, Cambridge, Massachusetts 02139, United States.

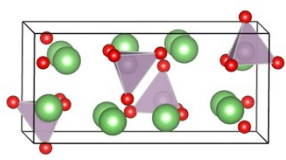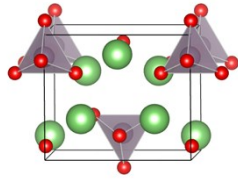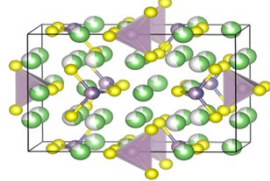[5]Materials Science and Technology Division, Oak Ridge National Laboratory, Oak Ridge, Tennessee 37831, USA.
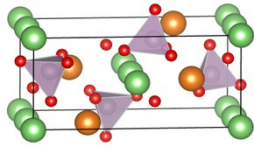
[6]Mechanical Engineering and Materials Science, Duke University, Durham, NC 27708, USA.

[7]Department of Chemical Science and Engineering, School of Materials and Chemical Technology, Interdisciplinary Graduate School of Science and Engineering, Tokyo Institute of Technology, 4259 Nagatsuta, Midori, Yokohama 226-8502, Japan

[8]Research Battery Technology, BMW Group, Munich 80788, Germany

Corresponding Author

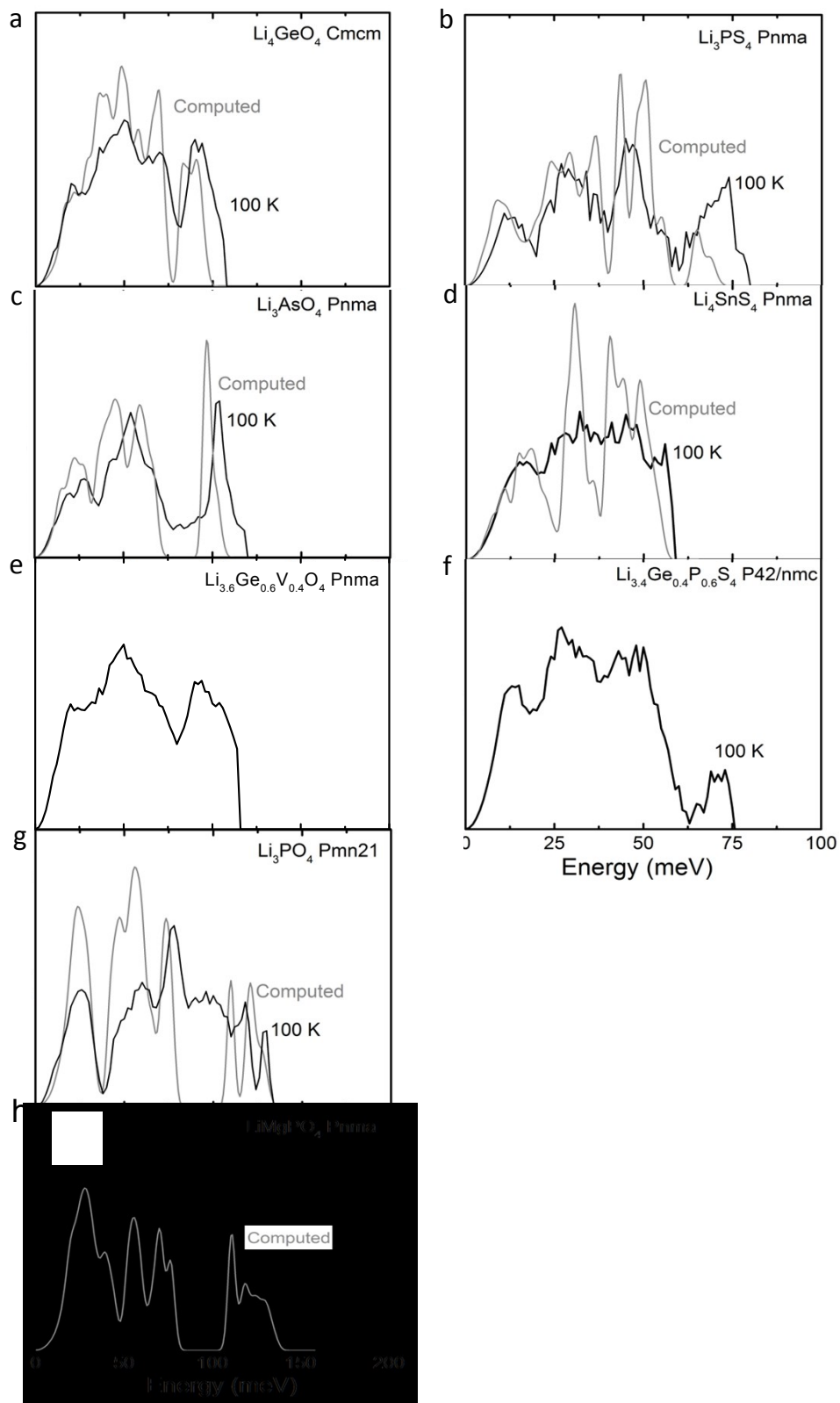- Yang Shao-Horn: shaohorn@mit.edu, Telephone: (617) 253-2259

	Compounds	Crystal structure
Lisicon Pnma	Li_3VO_4, Li_3PO_4, Li_3AsO_4, Li_3PS_4, Li_4GeS_4, Li_4SnS_4, Li_2CdSiO_4, Li_2MgGeO_4 $Li_{3.4}Ge_{0.4}P_{0.6}O_4$, $Li_{3.25}Ge_{0.25}P_{0.75}S_4$ and $Li_{3+x}Ge_xV_{1-x}O_4$ (x = 0.2, 0.4, 0.6, 0.8 and 1)	
Lisicon Pmn2₁	Li_3VO_4, Li_3PO_4, Li_3AsO_4, Li_3PS_4, Li_2CdGeO_4, Li_2CdGeS_4, $Li_2CdGeSe_4$, Li_2CdSiS_4 and Li_2CdSnS_4	
$Li_{10}GeP_2S_{12}$-like P4₂/nmc	$Li_{3.4}Ge_{0.4}P_{0.6}S_4$ and $Li_{10}SnP_2S_{12}$	
Olivine Pnma	$LiMgPO_4$, $LiMgAsO_4$, $LiMgVO_4$, $LiScSiO_4$, $LiInGeO_4$, $LiInSiO_4$	

Table S1. List of all compounds considered in this study, which include all the stoichiometric compositions of LISICON and Olivine without transition metal ions (except $LiCdPO_4$, $LiScGeO_4$ and $LiTmSiO_4$) listed in the Inorganic Crystal Structure Database (ICSD). LISICON structures have two phases: the low temperature (LT) phase with the space group Pmn2₁ and the high temperature phase (HT) with the space group Pnma. Total phonon densities of states (DOS) of some select LISICON compounds including Li_4GeO_4 (Cmcm), Li_3AsO_4 (Pnma), Li_3PO_4 (Pmn2₁), Li_3PS_4 (Pnma), Li_4SnS_4 (Pnma), $Li_{3.6}Ge_{0.6}V_{0.4}O_4$ (Pnma), $Li_{3.33}Sn_{0.33}P_{0.67}S_4$ (P4₂/nmc) and $Li_{3.4}Ge_{0.4}P_{0.6}S_4$

(P4$_2$/nmc) were measured with inelastic neutron scattering (INS) and are shown in Figure S1. The computed total as well as atom-projected phonon DOS of all the stoichiometric compounds in LISICON (both Pnma and Pmn2$_1$) and Olivine can be found in Figure S2. Compounds whose lithium conductivity was measured in this work (Li$_3$PO$_4$ (Pnma and Pmn2$_1$), Li$_3$VO$_4$ (Pmn2$_1$) LiMgPO$_4$ (Pnma), Li$_{3.4}$Ge$_{0.4}$P$_{0.6}$O$_4$ (Pnma), Li$_{3.4}$Ge$_{0.4}$P$_{0.6}$S$_4$ (P4$_2$/nmc) and Li$_{3+x}$Ge$_x$V$_{1-x}$O$_4$, where x = 0.2, 0.4, 0.6, 0.8 and 1) or prior work (Li$_3$PO$_4$ (Pnma)[1], LiMgPO$_4$ (Pnma)[2], Li$_3$VO$_4$ (Pmn2$_1$)[3], Li$_{3+x}$Ge$_x$V$_{1-x}$O$_4$ (Pnma, x = 0.2, 0.4, 0.6 and 0.8)[4], Li$_3$AsO$_4$ (Pnma)[5], Li$_3$PS$_4$ Pnm2$_1$[6] and Pnma[6], Li$_4$GeS$_4$,[7] Li$_4$SnS$_4$,[8] and Li$_{3.33}$Sn$_{0.33}$P$_{0.67}$S$_4$ [9]) and phonon DOS measured in this work are shown in green, compounds which are known in the ICSD but neither ionic conductivity nor phonon DOS were measured are shown in black, and finally structures that were computed only to complete the compositional series with known experimental data are shown in orange. For example, Li$_2$CdGeSe$_4$ were added to complete the anion substitution series of Li$_2$CdGeO$_4$ and Li$_2$CdGeS$_4$ known in the ICSD, Li$_2$CdSiS$_4$ were added to complete the cation substitution series of Li$_2$CdGeS$_4$ and Li$_2$CdSnS$_4$ known in the ICSD. LiMgVO$_4$ exists but has a different structure from Olivine. We include Olivine LiMgVO$_4$ that was computed only to compare with LiMgPO$_4$, which can be compared with parallel LISICON compounds of Li$_3$PO$_4$ and Li$_3$VO$_4$. The phonon DOS were computed using the finite displacement[10] method as implemented in Phonopy[11] using the force calculated from VASP.[12]
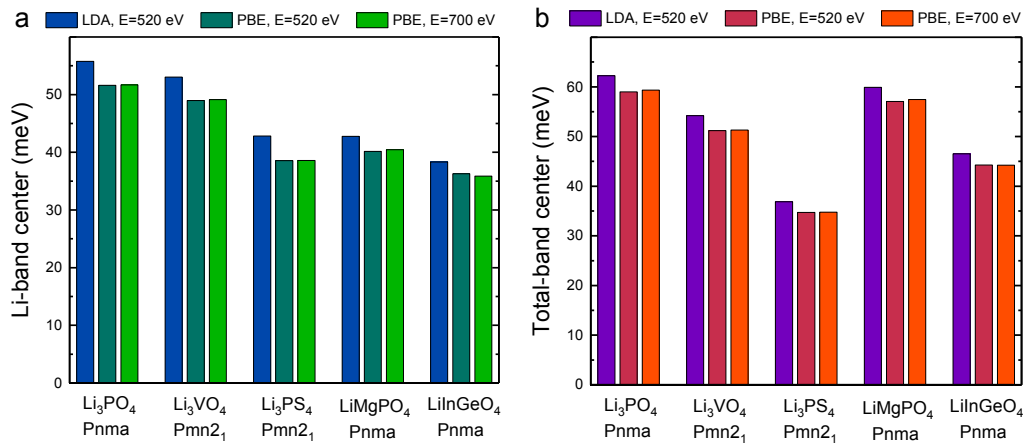
Figure S1. Comparison of a) computed Li-band center and b) computed total band center of some representative compounds in Lisicon and Olivine families using different functional and different cut-off energies for plane wave basis set.

a Li$_4$GeO$_4$ Cmcm
Computed
100 K

b Li$_3$PS$_4$ Pnma
Computed
100 K

c Li$_3$AsO$_4$ Pnma
Computed
100 K

d Li$_4$SnS$_4$ Pnma
Computed
100 K

e Li$_{3.6}$Ge$_{0.6}$V$_{0.4}$O$_4$ Pnma

f Li$_{3.4}$Ge$_{0.4}$P$_{0.6}$S$_4$ P42/nmc
100 K

g Li$_3$PO$_4$ Pmn21
Computed
100 K

h LiMgPO$_4$ Pnma
Computed

Energy (meV)

0   25   50   75   100
Energy (meV)

Figu

re S2. Comparison between the total phonon DOS measured (at 100K) with INS and

computed with DFT of LISICONs **a**, Li_4GeO_4 (Cmcm) **b**, Li_3PS_4 (Pnma) **c**, Li_3AsO_4 (Pnma) **d**, Li_4SnS_4 (Pnma) **e**, $Li_{3.6}Ge_{0.6}V_{0.4}O_4$ (Pnma) **f**, $Li_{3.4}Ge_{0.4}P_{0.6}S_4$ (P4_2/nmc) **g**, Li_3PO_4 (Pmn2_1) and **h**, Olivine LiMgPO4 (Pnma). For Li_3PO_4 (Pmn2_1), it was difficult to remove all of the water from the sample, which resulted in a large background scattering, which resulted in nonzero intensities at ~100 meV. A higher constant fraction (0.8) during analysis of the sample was used. For $Li_{3.33}Sn_{0.33}P_{0.67}S_4$ (P4_2/nmc) and $Li_{3.4}Ge_{0.4}P_{0.6}S_4$ (P4_2/nmc) the phonon DOS at 0 K couldn't be obtained due to presence of imaginary modes. Experimental phonon DOS were measured by INS at the Spallation Neutron Source at Oak Ridge National Laboratory while the computed spectra were calculated using the finite displacement method[10] as implemented in Phonopy[11] using the force calculated from VASP.[12] The Sensitivity of the measured phonon DOS to reduction parameters were examined and the details for Li_3PO_4 Pnma at 10 K are shown in Figure S3. A systematic red shift of the high energy features in the computed phonon DOS with respect to the measured phonon DOS can be partially attributed to a well known issue of overestimated lattice parameters associated with GGA functional (PBE).[13]
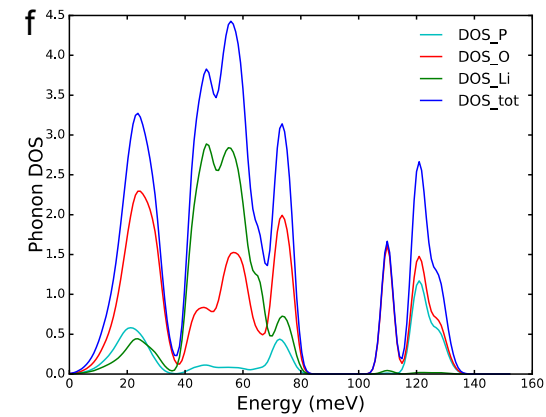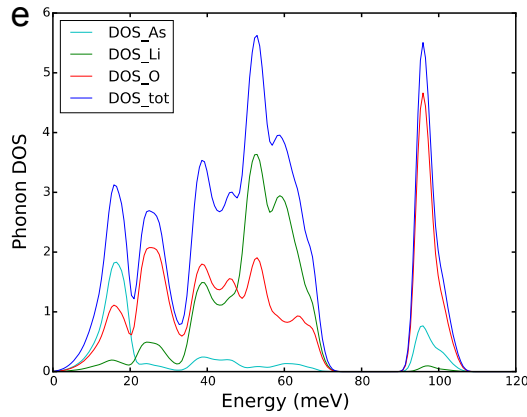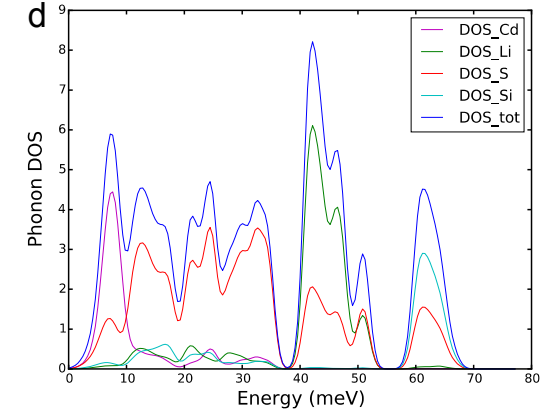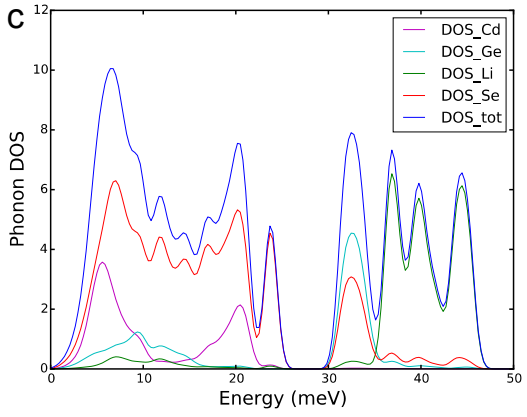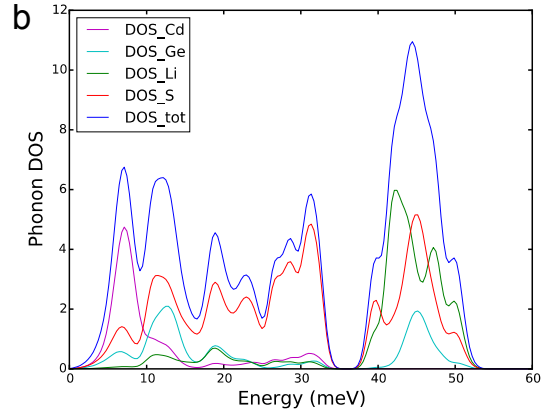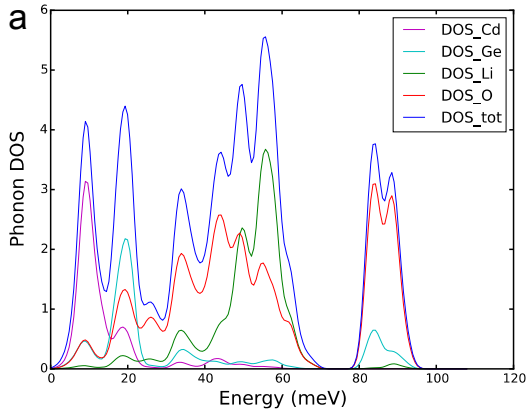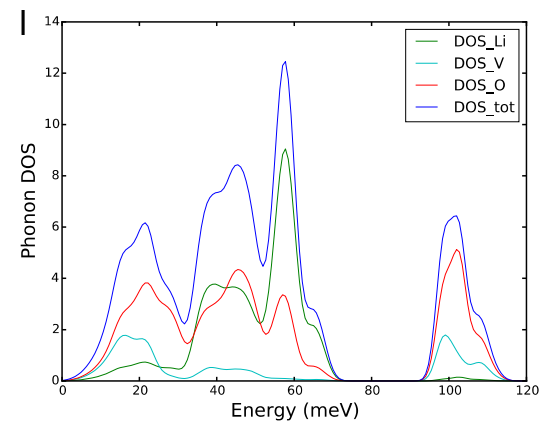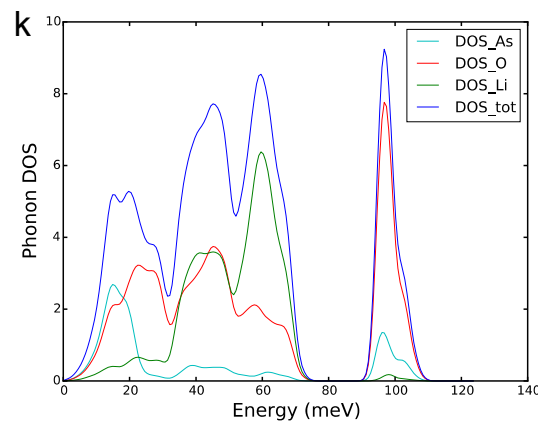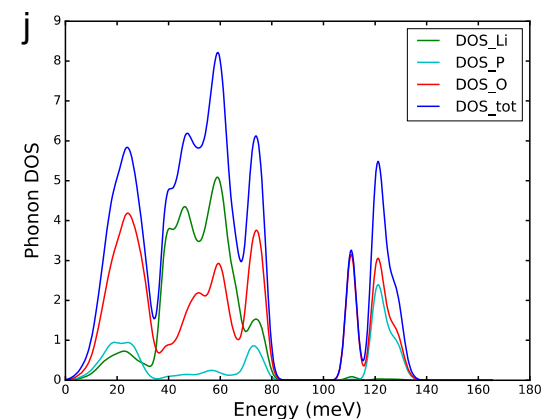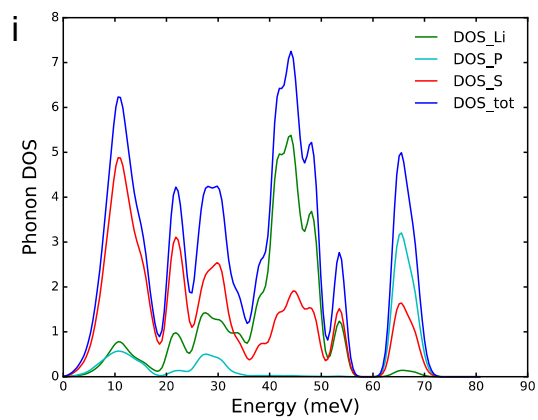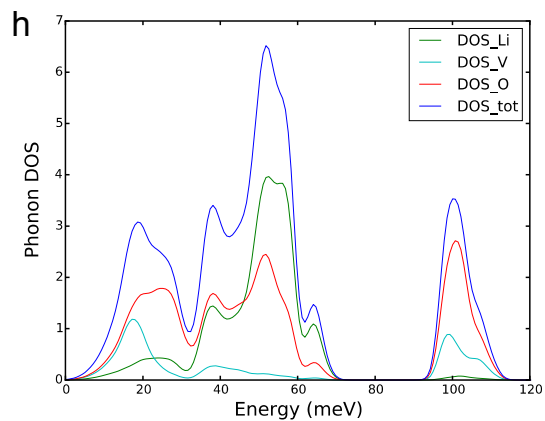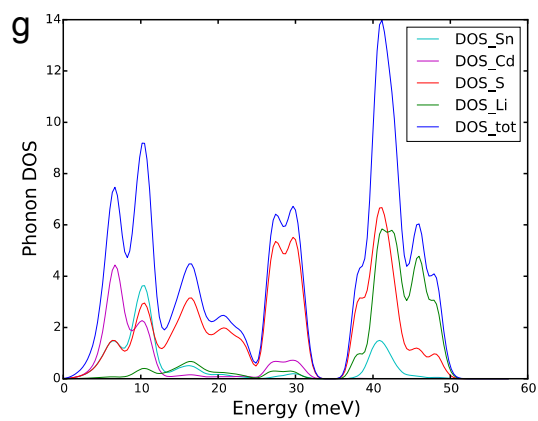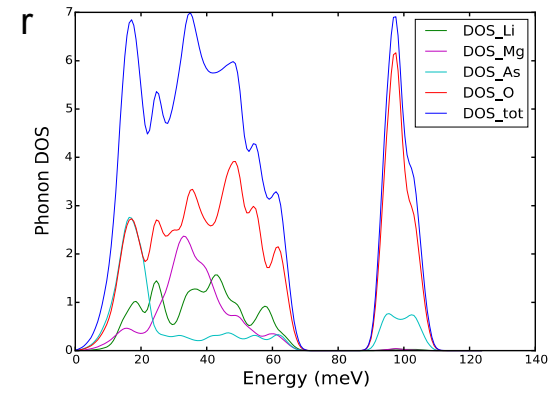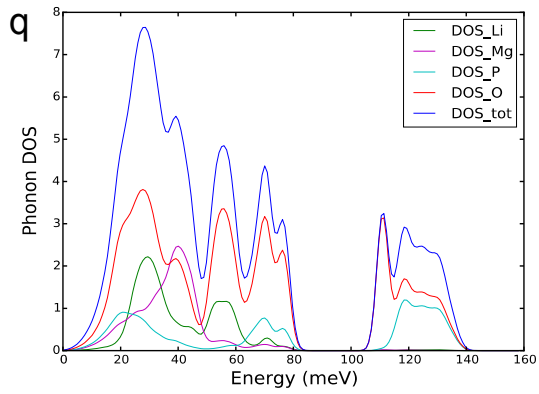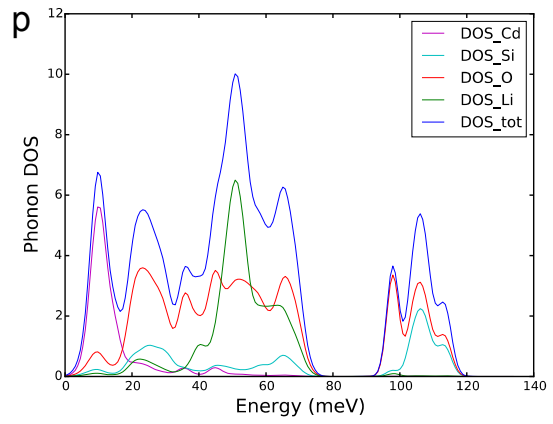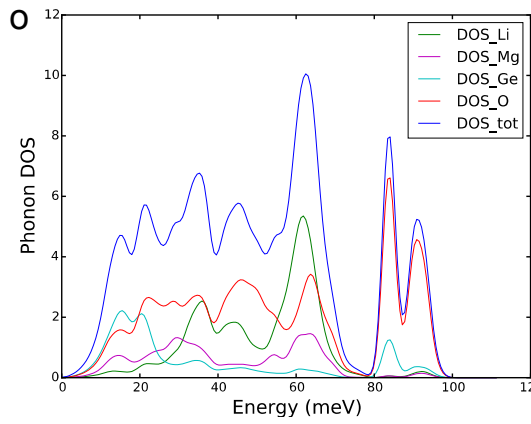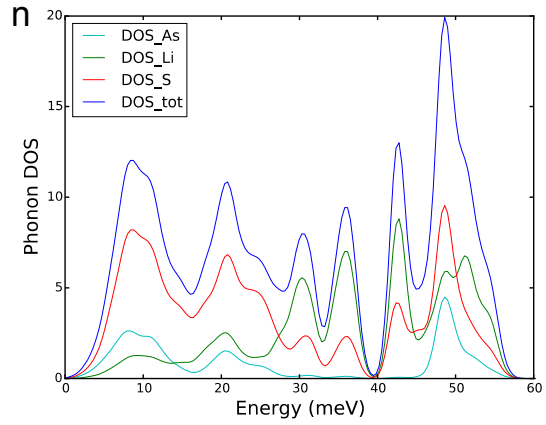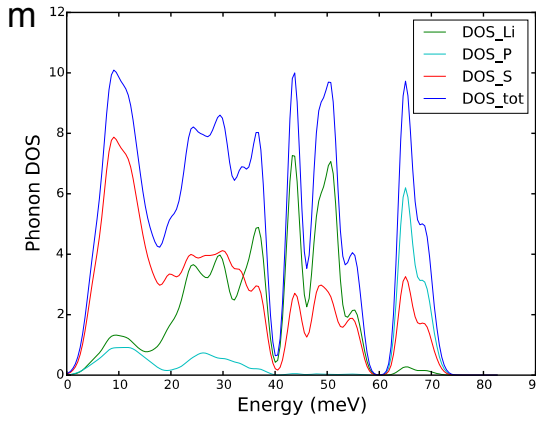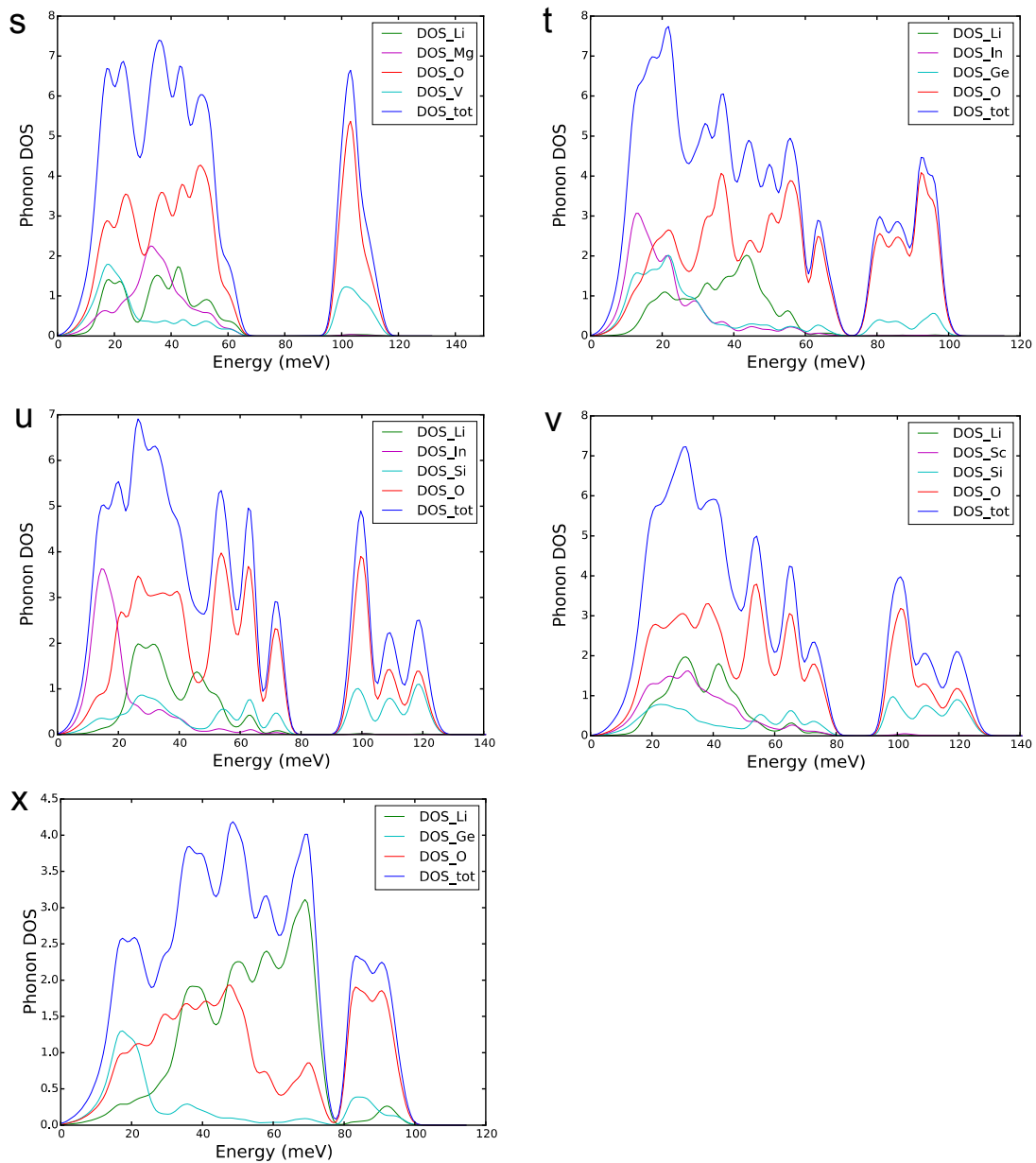
Figure S3. Computed total as well as atom-projected density of state of all LISICON *Pmn2₁* compounds **a,** Li_2CdGeO_4 **b,** Li_2CdGeS_4 **c,** $Li_2CdGeSe_4$ **d,** Li_2CdSiS_4 **e,** Li_3AsO_4 **f,** Li_3PO_4 **g,** Li_2CdSnS_4 **h,** Li_3VO_4 **i,** Li_3PS_4 ;LISICON *Pnma* **j,** Li_3PO_4 **k,** Li_3AsO_4 **l,** Li_3VO_4 **m,** Li_3PS_4 **n,** Li_3AsS_4 **o,** Li_2MgGeO_4 **p,** Li_2CdSiO_4 ;Olivines *Pnma* **q,** $LiMgPO_4$ **r,** $LiMgAsO_4$ **s,** $LiMgVO_4$ **t,** $LiInGeO_4$ **u,** $LiInSiO_4$ **v,** $LiScSiO_4$ and **x.** Li_4GeO_4 (Cmcm). Notice that the structure of Li_4GeO_4 is different from LISICON and olivine. The phonon

DOS were computed using the finite displacement[10] method as implemented in Phonopy[11] using the force calculated from VASP.[12]
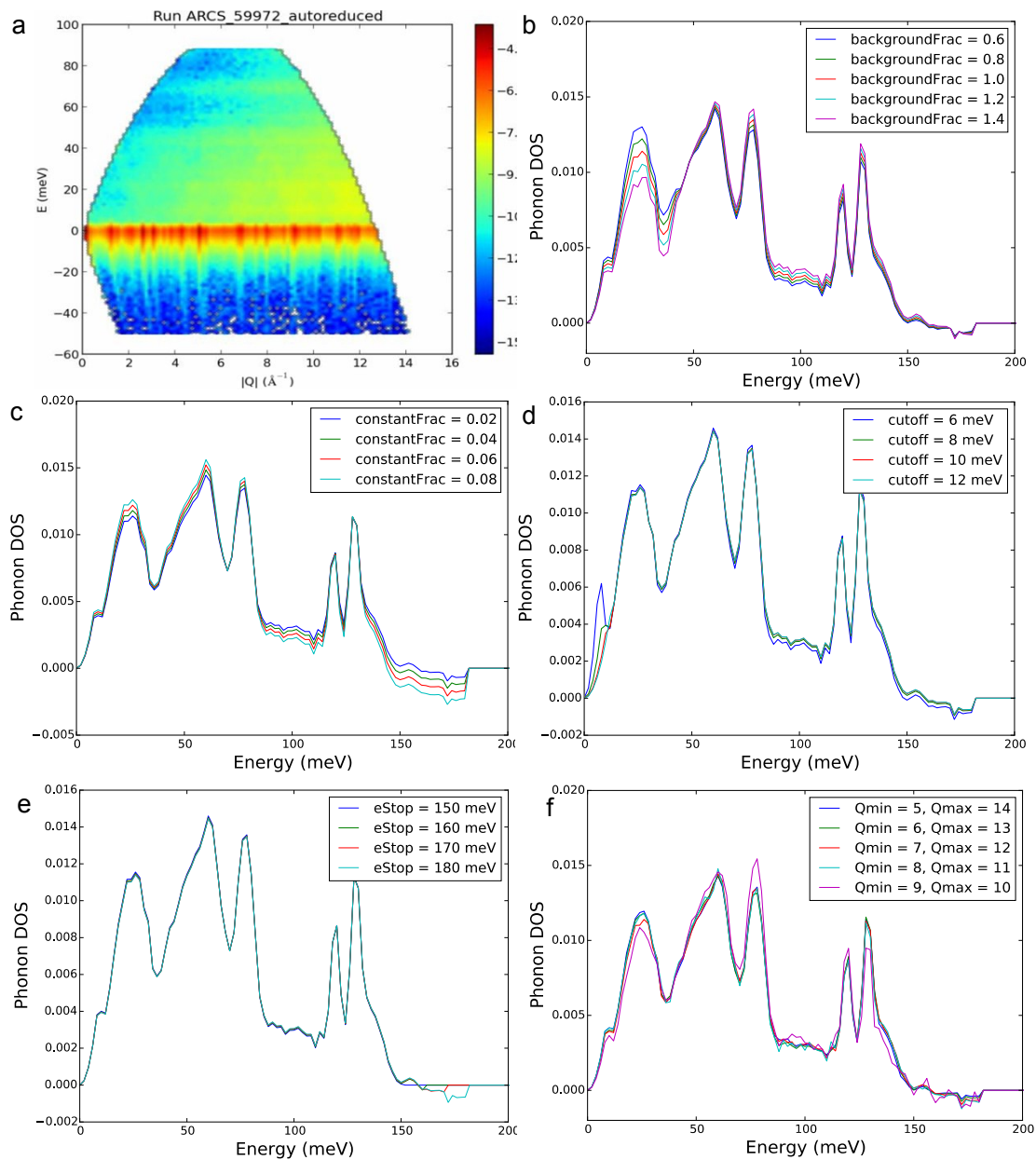
Figure S4 Sensitivity of phonon density-of-states to reduction parameters for Li_3PO_4 Pnma at 10 K. Five parameters with the most significant effects are shown. For each plot we fix all the parameters except one, which was varied systemically to examine its influence on the reduced data. a) The scattering function $S(|q|, \omega)$, which are the raw data

and are directly proportional to neutron count recorded by the detector. The intense red feature around 0 meV is due to elastic scattering. b) Background fraction (the typical value of this parameter is 1), c) constant fraction. The value of this parameter is chosen such that the intensity above the highest frequency is as close to zero as possible. d) Cutoff. This parameter is used to remove the elastic peak near the origin. e) eStop is the energy cutoff above which the intensity is set to zero, its values depend on the highest frequency of the material and can be guessed reliably from the spectra. f) Range in the magnitude of the wave vector (q_{min}-q_{max}) in $Å^{-1}$, over which we integrate the scattering function to generate the DOS.
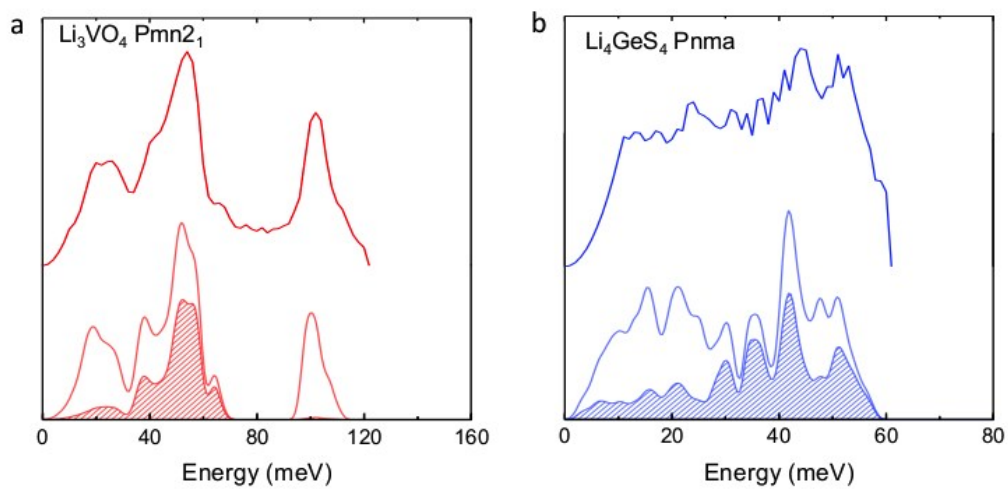
Figure S5. Measured and computed total phonon density of states as well as Li-projected DOS of a, Li_3VO_4 $Pmn2_1$ and b, Li_4GeS_4 Pnma. The main effect of isovalent substitution is to shift the high-energy feature without altering significantly the overall DOS.
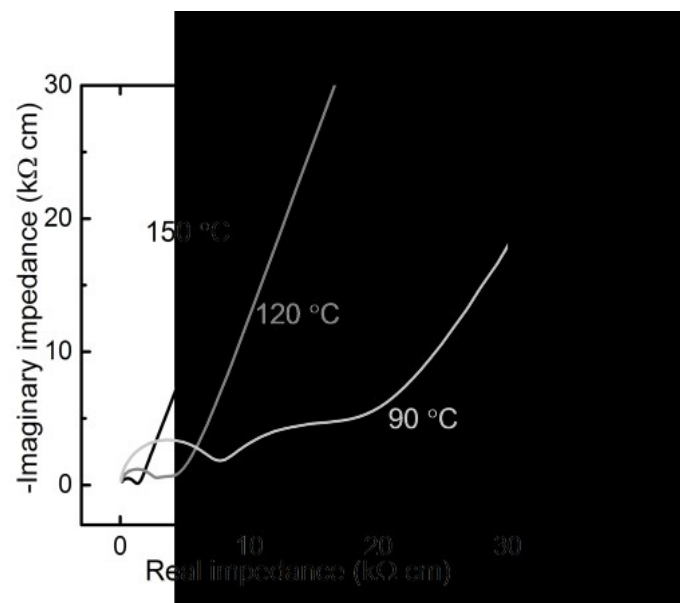
Figure S6. Experimental values from impedance spectroscopy of $Li_{3.2}Ge_{0.2}V_{0.8}O_4$ at select temperatures. For conductivity measurements, the powders were pressed at 1 GPa into pellets with a 6 mm diameter and were approximately 1-1.5 mm thick. The pellets were then sintered at 800 °C for 10 hrs using a ramp rate of 5 °C/min and then were polished before being sputtered with 100 nm of gold on each face of the pellet. Impedance was measured at frequencies between 7 MHz and 0.1 Hz. Our measured activation of 1.1 eV for Li_3PO_4-Pnma, 1.02 eV for Li_3VO_4-Pmn2_1, 0.5 eV for $Li_{3.4}Ge_{0.4}P_{0.6}O_4$-Pnma, 0.96 eV for $LiMgPO_4$ and ~0.4 - 0.6 eV for $Li_{3+x}Ge_xV_{1-x}O_4$, where x = 0.2, 0.4 and 0.6 are in good agreements with previously reported values.[2,3,4,14]
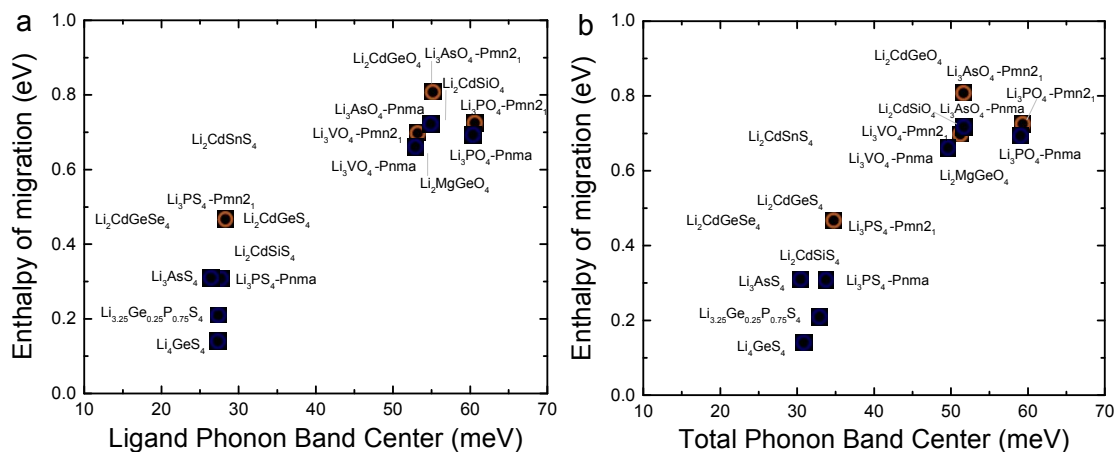
Figure S7. Computed enthalpy of migration versus a) computed ligand band center and b) computed total band center of stoichiometric LISICONs and substituted LISICON $Li_{3.25}Ge_{0.25}P_{0.75}S_4$. All the band centers were determined from the computed phonon DOS at 0 K. All the computed enthalpies of migration were calculated using the standard climbing image nudge elastic band method[15] and the phonon band center is defined as the average phonon frequency weighted by phonon DOS. The blue and orange colors refer to the HT phase (space group Pmna) and the LT phase (space group Pmn2$_1$), respectively. Li_4GeO_4 (Cmcm) was not included in this graph as it does not have the LISICON structure nor lithium migration pathway similar to that used for LISICON. The filled circles are compounds that are known in the ICSD and/or computed in this work, where the lithium ion conductivity has not been measured experimentally. For more details, please refer to Table S1.
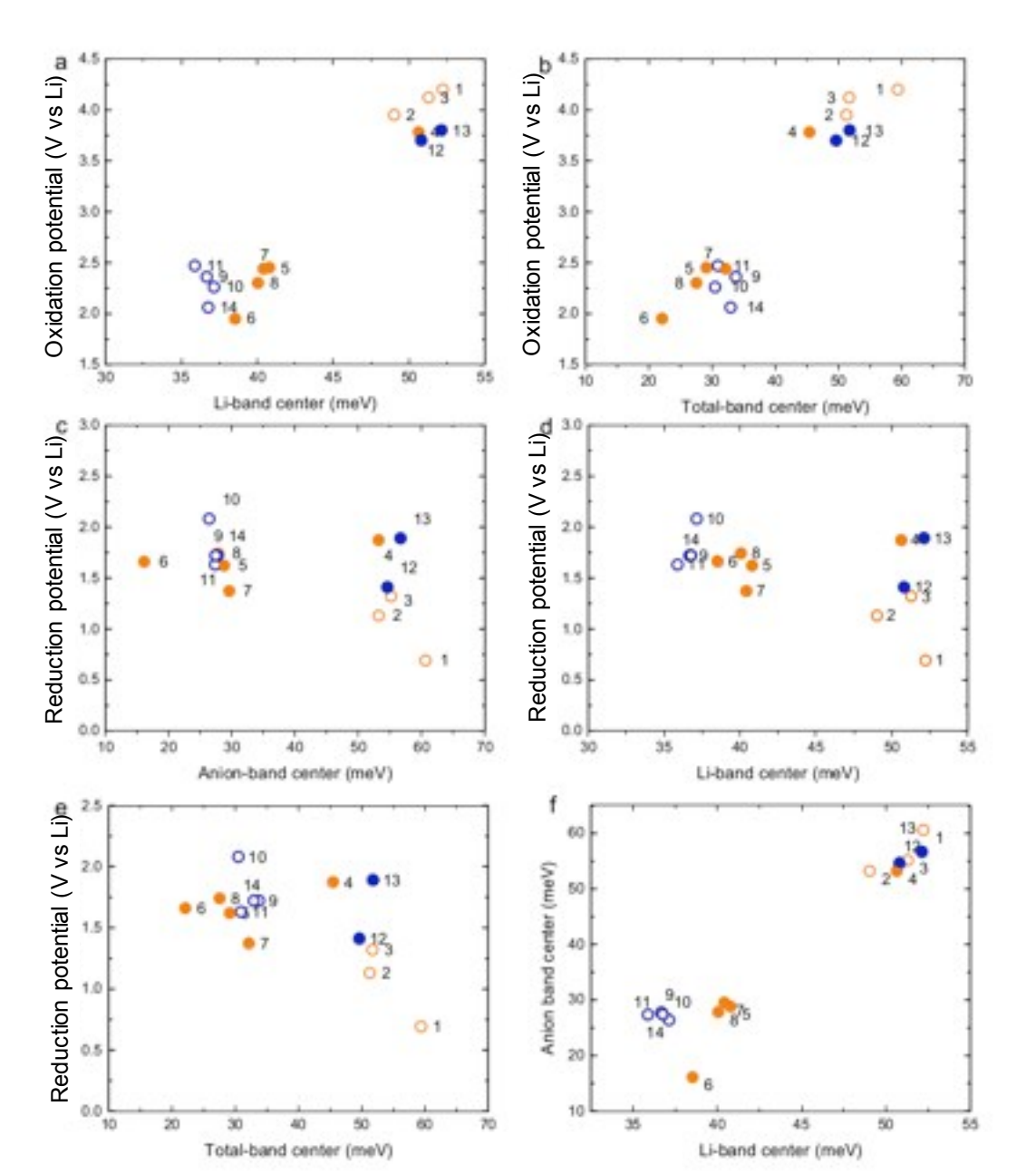
Figure S8 Correlations between the oxidation potential and a) computed Li-band center b) computed total-band center. Absence of correlation between reduction potential and c) Anion-band center, d) Li-band center and e) total band center. f) The downshifting of anion band center is broadly accompanied by the downshifting of Li-band center. The numbers in the plots refer to: 1. Li_3PO_4 2. Li_3VO_4 3. Li_3AsO_4 4. Li_2CdGeO_4 5.

Li$_2$CdGeS$_4$ 6. Li$_2$CdGeSe$_4$ 7. Li$_2$CdSiS$_4$ 8. Li$_2$CdSnS$_4$ 9. Li$_3$PS$_4$ 10. Li$_3$AsS$_4$ 11. Li$_4$GeS$_4$ 12. Li$_2$MgGeO$_4$ 13. Li$_2$CdSiO$_4$ and 14. Li$_{3.25}$Ge$_{0.25}$P$_{0.75}$S$_4$. The stability window was computed by constructing the grand potential phase diagram and by varying the chemical potential of Li until the grand potential of the electrolytes are above the convex hull.[16] The blue and orange colors refer to the HT phase (space group Pmna) and the LT phase (space group Pmn21) respectively. The filled circles are compounds that are known in the ICSD and/or computed in this work, where the lithium ion conductivity has not been measured experimentally. For more details, please refer to Table S1.
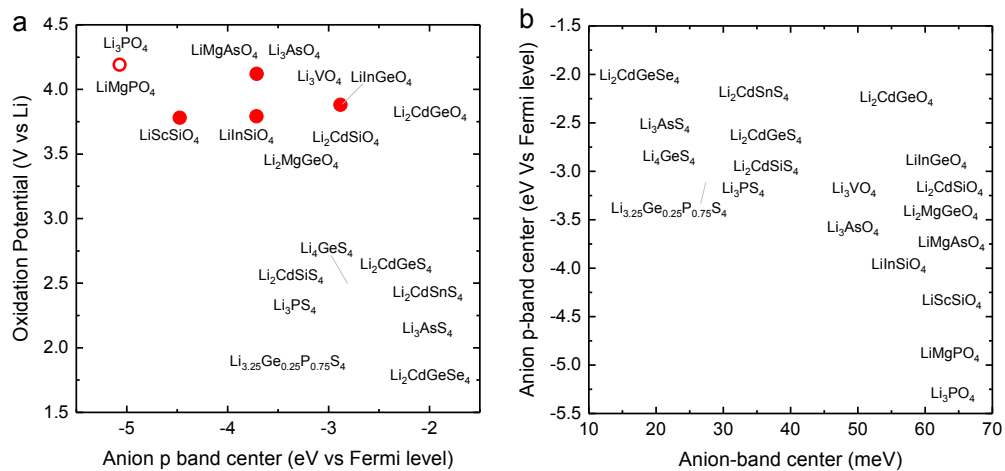
Figure S9. Absence of correlation between a) oxidation potential and anion p-band center b) Anion p-band center and anion phonon band center.
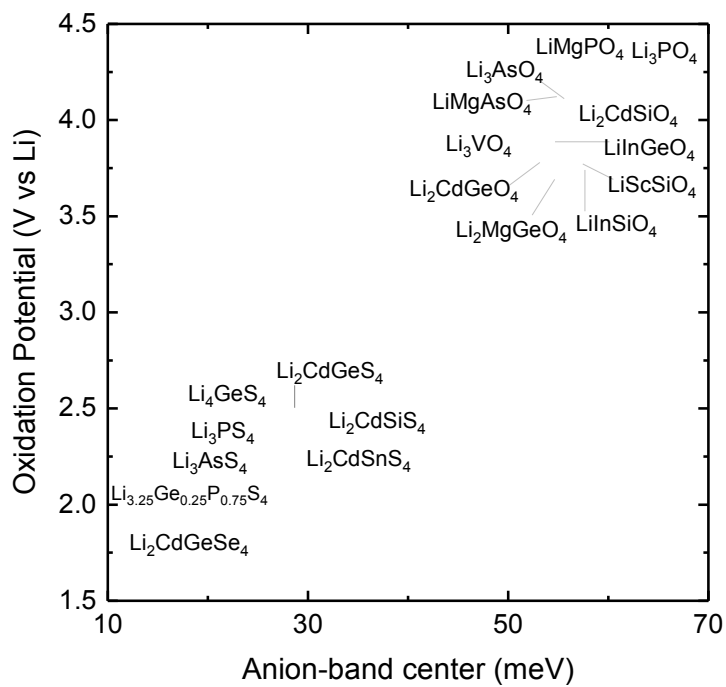
Figure S10. Correlation between oxidation potential of Lisicon and Olivine compounds and their anion-band center.
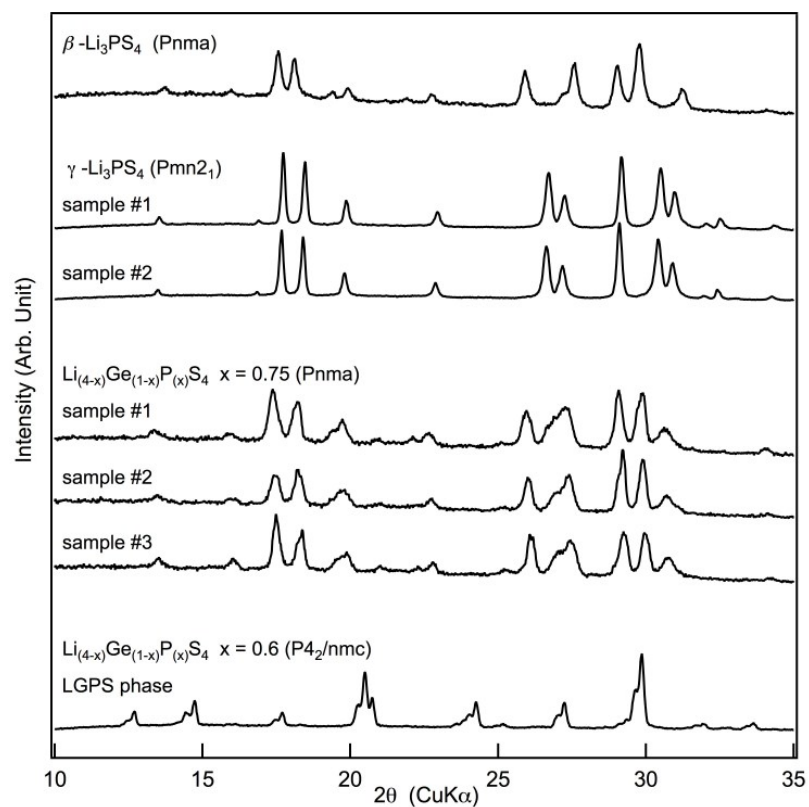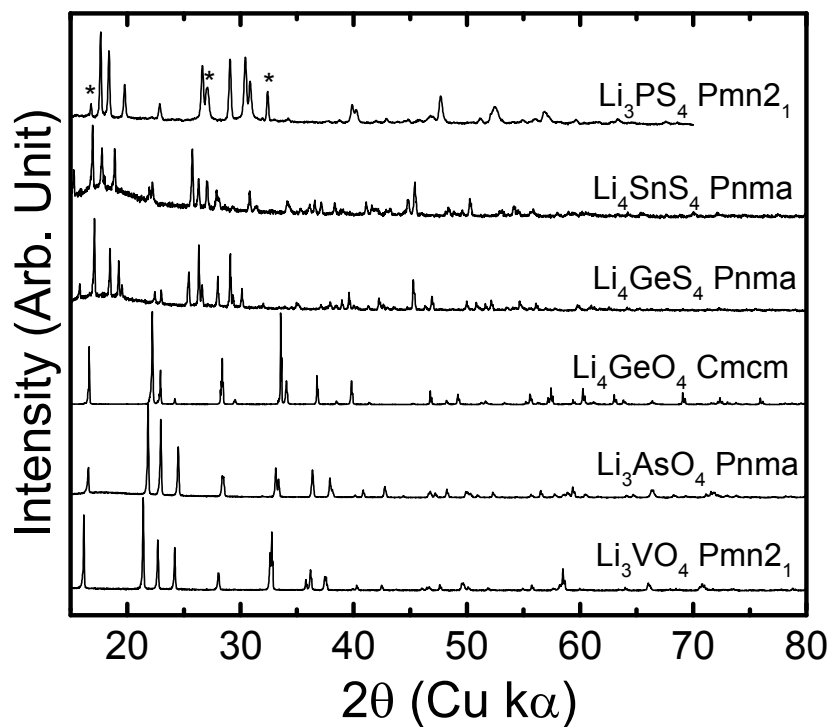
Figure S11 XRD spectra of all compound measured in this study. Most samples were phase pure, impurity peaks are identified with an asterisk (*). a) XRD spectra of Li_4SnS_4,

Li_4GeS_4, Li_3PS_4, $LiMgPO4$ and Li_3AsO_4. For Li_4SnS_4 and Li_4GeS_4, amorphous hump at low angles is from the plastic dome of the sealed cell that is used to measure the reactive sulfides. The main impurity phase in Li_3PS_4 is Li_2PS_3 b) Diffraction pattern for $Li_{(4-x)}Ge_{(1-x)}V_xO_4$ compared to reference patterns. Labels of solid solution have the percentage of vanadium noted (V20 corresponds to x=0.2). c) Diffraction pattern for $Li_{(4-x)}Ge_{(1-x)}P_xS_4$. For phonon DOS measurements, for Li_3PS_4 ($Pmn2_1$) sample 1 and 2 were mixed, and for $Li_{3.25}Ge_{0.25}P_{0.75}S_4$ (Pnma) samples $1 - 3$ were mixed. Minute Li_2PS_3 impurity can be found in Li_3PS_4 samples.

Materials Synthesis

For neutron inelastic scattering measurements, the materials were synthesized through solid-state synthesis methods. Appropriate mixtures (5-10% excess lithium for Li_3PO_4, Li_4GeO_4, $Li_{3.4}Ge_{0.4}P_{0.6}O_4$, $Li_{3.6}Ge_{0.6}V_{0.4}O_4$, and $Li_{3.8}Ge_{0.8}V_{0.2}O_4$ and stoichiometric mixtures in all other cases) of Li_2CO_3 (99.998% Alfa Aesar), $(NH_4)_2HPO_4$ (98% Strem Chemicals), V_2O_5 (>99.6% trace metal basis, Aldrich), GeO_2 (>99.99% trace metal basis, Aldrich), and MgO (99.95%, Alfa Aesar) were ground with a mortar and pestle or mixed overnight in ethanol. The resulting powders were calcined in dry air at 800 °C for 20 hours (10 hours for Li_4GeO_4, Li_3VO_4, and Li_3PO_4) using a ramp rate of 5 °C/min on heating and cooling to produce the desired material. The details for the synthesis of sulfide compounds can be found in the SI and the XRD spectra can be found in Figure S9.

Li_3PO_4 (Pmn21) was obtained from Sigma Aldrich and was heated under vacuum to remove moisture before use. Appropriate mixtures (5% excess Li for Li_3PO_4 and $Li_{3.2}Ge_{0.2}P_{0.8}O_4$, and stoichiometric mixtures in all other cases) of Li_2CO_3 (99.998% Alfa Aesar), $(NH_4)_2HPO_4$ (98% Strem Chemicals), V_2O_5 (>99.6% trace metal basis, Aldrich) and GeO_2 (>99.99% trace metal basis, Aldrich) were ground with a mortar and pestle. The resulting powders were calcined in dry air at 800 °C for 10 hrs using a ramp rate of 5 °C/min to produce the desired material. These powders were pressed at 1 GPa into pellets with a 6 mm diameter and were approximately 1-1.5 mm thick. The pellets were then sintered at 800 °C for 10 hrs using a ramp rate of 5 °C/min for cooling and heating, and then were polished before being sputtered with 100 nm of gold on each face of the pellet. Lithium phosphate doped with 40% lithium vanadate required an additional calcination at 900 °C to achieve a solid solution of lithium vanadate and lithium phosphate, before the powders were sintered at the previously described sintering conditions.

Synthesis preparation steps of sulfur-based conductors were performed under an argon atmosphere. The starting materials used for the synthesis of γ-Li_3PS_4 (Pmn21) consisted of Li_2S

(>99% purity, Mitsuwa Chemical) and P_2S_5 (>99% purity, Sigma Aldrich). These reagents were weighted in the appropriate molar ratio and mixed by planetary ball milling for 20 h. The specimens were then pressed into pellets, sealed in a quartz tube at 10 Pa, and heated at 500 °C for 8 h, which was slowly cooled to room temperature. For β-Li_3PS_4 (Pnma) the Li_2S powder was milled to obtain fine particles using a ball-milling apparatus. All of the procedures were conducted under an argon atmosphere. Starting materials were weighed in the appropriate molar ratio and mixed by planetary ball milling for 40 h. The samples were then pressed into pellets, sealed in a quartz tube at 10 Pa, and heated at 300 °C for 8 h, which was cooled slowly to room temperature. For $Li_{4-x}Ge_{1-x}P_xS_4$ ($x = 0.75$, Pnma) the starting materials used for the synthesis were Li_2S (>99% purity, Mitsuwa Chemical) and P_2S_5 (>99% purity, Sigma Aldrich), and GeS_2 (>99.99% purity, Kojundo Chemical Laboratory). These powder samples were weighed in the appropriate molar ratio and mixed for 30 min using a vibrating mill (CMT, Tl-100). The samples were then pressed into pellets, placed into a carbon crucible, and then sealed at 10 Pa in a carbon-coated quartz tube. After being heated at a reaction temperature of 750 °C for 8 h, which was quenched subsequently in ice water. $Li_{3.4}Ge_{0.4}G_{0.6}S_4$ ($P4_2$/nmc) was prepared according to previous work.[17] Li_4GeS_4 was synthesized by reacting stoichiometric ratios of Li_2S (Alfa Aesar 99.9% metal basis) and GeS_2 (Santa Cruz Biotechnology) at 700 °C for 8 h followed by a 12 hour cooling to room temperature under argon. Li_4SnS_4 was synthesized by reacting stoichiometric ratios of Li_2S (Alfa Aesar 99.9% metal basis) and SnS_2 (Santa Cruz Biotechnology) at 700 °C for 8 h followed by a 12-hour cooling to room temperature under argon. $Li_{3.33}Sn_{0.33}P_{0.67}S_4$ ($P4_2$/nmc, NEI Corporation) was used as purchased. Phase purity was confirmed by X-ray diffraction (Figure S11) measured on a Panalytical X'Pert Pro, Rigaku Smartlab, or Rigaku MiniFlex300 diffractometers with Cu k-alpha sources. All sulfur-based samples were stored under inert atmosphere until immediately before measuring the phonon density of states at Oak Ridge National Laboratory.

References

1. Hu, Y.-W., Raistrick, I. D. & Huggins, R. A. Ionic conductivity of lithium phosphate-doped lithium orthosilicate. *Mater. Res. Bull.* **11,** 1227–1230 (1976).

2. Enciso-Maldonado, L. *et al.* Computational Identification and Experimental Realization of Lithium Vacancy Introduction into the Olivine $LiMgPO_4$. *Chem. Mater.* **27,** 2074–2091 (2015).

3. Mishra, K. M., Lal, A. K. & Haque, F. Z. Ionic and electronic conductivity in some alkali vanadates. *Solid State Ion.* **167,** 137–146 (2004).

4. Rodger, A., Kuwano, J. & West, A. Li+ Ion Conducting Gamma-Solid Solutions in the Systems Li_4XO_4-Li_3YO_4 - X = Si, Ge, Ti ; Y = P, As, V ; Li_4XO_4-$LiZO_2$-Z = Al, Ga, Cr and Li_4GeO_4-Li_2CaGeO_4. *Solid State Ion.* **15,** 185–198 (1985).

5. Khorassani, A. & West, A. New Li^+ Ion Conductors in the System Li_4SiO_4-Li_3AsO_4. *Solid State Ion.* **7,** 1–8 (1982).

6. Tachez, M., Malugani, J.-P., Mercier, R. & Robert, G. Ionic conductivity of and phase transition in lithium thiophosphate Li_3PS_4. *Solid State Ion.* **14,** 181–185 (1984).

7. Sahu, G. *et al.* A high-conduction Ge substituted Li_3AsS_4 solid electrolyte with exceptional low activation energy. *J. Mater. Chem. A* **2,** 10396–10403 (2014).

8. Sahu, G. *et al.* Air-stable, high-conduction solid electrolytes of arsenic-substituted Li_4SnS_4. *Energy Environ. Sci.* **7,** 1053–1058 (2014).

9. Bron, P. *et al.* $Li_{10}SnP_2S_{12}$: An Affordable Lithium Superionic Conductor. *J. Am. Chem. Soc.* **135,** 15694–15697 (2013).

10. Parlinski, K., Li, Z. Q. & Kawazoe, Y. First-Principles Determination of the Soft Mode in Cubic ZrO_2. *Phys. Rev. Lett.* **78,** 4063–4066 (1997).

11. Togo, A. & Tanaka, I. First principles phonon calculations in materials science. *Scr. Mater.* **108,** 1–5 (2015).

12. Kresse, G. & Furthmüller, J. Efficient iterative schemes for *ab-initio* total-energy calculations using a plane-wave basis set. *Phys. Rev. B* **54,** 11169–11186 (1996).

13. Perdew, J. P., Burke, K. & Ernzerhof, M. Generalized Gradient Approximation Made Simple. *Phys. Rev. Lett.* **77,** 3865–3868 (1996).

14. Hu, Y.-W., Raistrick, I. D. & Huggins, R. A. Ionic Conductivity of Lithium Orthosilicate—Lithium Phosphate Solid Solutions. *J. Electrochem. Soc.* **124,** 1240–1242 (1977).

15. Henkelman, G., Uberuaga, B. P. & Jónsson, H. A climbing image nudged elastic band method for finding saddle points and minimum energy paths. *J. Chem. Phys.* **113,** 9901–9904 (2000).

16. Richards, W. D., Miara, L. J., Wang, Y., Kim, J. C. & Ceder, G. Interface Stability in Solid-State Batteries. *Chem. Mater.* **28,** 266–273 (2016).

17. Kamaya, N. *et al.* A lithium superionic conductor. *Nat. Mater.* **10,** 682–686 (2011).